Master's Thesis of Science

Unidirectional Real-Time Photoswitching of Diarylethene Molecular Junctions with Multilayer Graphene Electrodes

다층 그래핀 전극을 가지는 Diarylethene 분자 접합의 실시간 단향성 광스위칭

February 2019

Graduate School of Physics and Astronomy
Seoul National University
Physics Major

Jeongmin Koo

Unidirectional Real-Time Photoswitching of Diarylethene Molecular Junctions with Multilayer Graphene Electrodes

Supervised by Professor Takhee Lee

Submitting a master's thesis of Public Administration

January 2019

Graduate School of Physics and Astronomy
Seoul National University
Physics Major

Jeongmin Koo

Confirming the master's thesis written by
Jeongmin Koo
August 2018

Chair	Seunghun Hong	(Seal)
Vice Chair	Takhee Lee	(Seal)
Examiner	Dai-Sik Kim	(Seal)

Abstract

Photoswitching characteristics of diarylethene (DAE) self-assembled monolayers (SAMs) were studied by using a vertical molecular junction structure consisting of Au and multilayer graphene (MLG) as a bottom and top electrode. The DAE molecular junctions showed two stable electrical states, a closed state (high conductance) or an open state (low conductance), which are created upon illumination with UV or visible light, respectively. For the Au-DAE-MLG junction structure, I observed that the current levels between the two conductance states were separated by two orders of magnitude. However, in a real-time measurement, I observed only unidirectional switching behavior from the open to the closed state unlike the Au-DAE-reduced graphene oxide (rGO) molecular junctions which showed reversible photoswitching behavior in a previous study. At the same time, the Au-DAE-MLG molecular junctions showed a significantly reduced switching time, about 10 min, whereas the Au-DAE-rGO molecular junctions showed the switching time that was closed to almost an hour. To explain these results, I made simple assumptions and utilized the Landauer formula to the two kinds of molecular junctions. This analytical method reproduced the experimental current-voltage curves well, and the coupling parameters representing the interaction of DAE molecule and MLG top electrode were extracted. As a result, large coupling values appeared for the Au-DAE-MLG molecular junctions and small coupling values for the Au-DAE-rGO molecular junctions. The strong interaction between the DAE molecule and MLG electrode quenched the molecular photoswitching phenomena. On the other hand, the weak interaction, a small coupling value, enableds the Au-DAE-rGO molecular junctions to switch reversibly. The validity of this interpretation is supported by theoretical calculations of the electrode-molecule coupling strength based on the Landauer formula.

Keyword : molecular electronics, photoswitching, diarylethene, self-assembled monolayer, graphene electrode
Student Number : 2015-22586

Table of Contents

List of Figures

List of Table

Chapter 1. Introduction

1.1. Diarylethene Photoswitching Junctions in Molecular Electronics

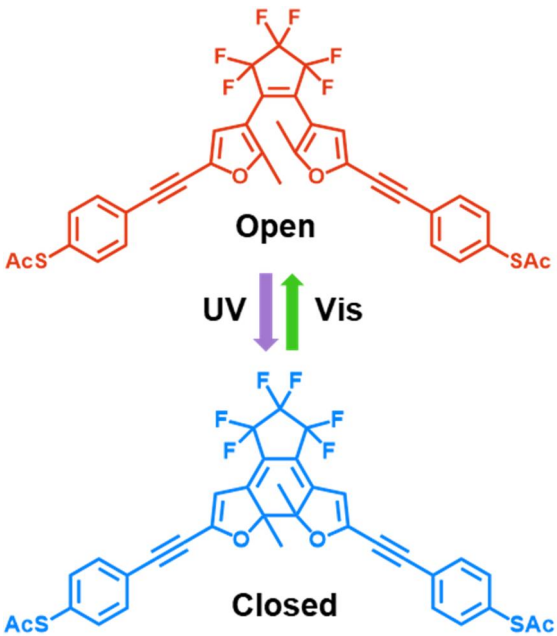

Fig. 1 The chemical structures of the DAE molecule in the open (top) and closed (bottom) state.

To achieve the ultimate miniaturization of electronic devices, a wide range of studies in the field of molecular electronics has been carried out over the last decades. Important developments include utilization of functional molecules for realizing molecular wires, rectifiers, switches, transistors, and thermoelectric devices [1-10]. Among such developments, the molecular switch is a promising building block due to its potential as a memory device. Usually, a molecular switch consists of two stable isomers and undergoes a transition between them upon exposure to an external stimulus such as light, heat, or an electric field [11-13]. In particular, light is useful for switching devices because of its addressability and compatibility with solid-state device structures. Therefore, the design of photochromic molecules is important for molecular switching devices. DAEs form

a class of photochromes with two different conductance states, i.e., a high conductance (closed; ON) and a low conductance (open; OFF) state. In solution, DAEs can be converted between these two states by illumination with UV or visible light, respectively. This property makes them good candidates for photoswitching devices due to a large conductance difference between the two states and their response to light [14-16].

1.2. Various Photoswitching Phenomena in Single-Molecular Junctions.

As promising photoswitching molecules, DAEs have been utilized in various ways with the aim to demonstrate bidirectional switching in molecular devices. For an Au-DAE-Au junction, only a unidirectional switching from the closed to the open state has been observed [17]. According to a theoretical study, this result is attributed to the quenching of the excited state of the DAE due to strong electronic coupling between the Au metal and the sulfur-based end group, thereby hindering the molecule to adopt its high conductance state [18]. On the other hand, unidirectional switching from the low- to the high-conductance state in Au-DAE-Au single-molecule junctions was obtained by modifying the side-arms and end-groups such that they form rigid conjugated molecular wires [19]. These molecules feature a very high quantum yield for the ON switching reaction, but a relatively low one for the OFF switching, explaining the inversed unidirectional switching. In addition, a similar single DAE molecule, bridged between carbon nanotubes [15] or graphene sheets, [20] showed a unidirectional switching from the open to the closed state, because strong molecule-electrode couplings between closed state DAE and graphene electrodes enabled the energy transfer from the photoexcited molecule to the extended π-electron system in the electrodes [7, 20]. To overcome this unidirectional switching in DAE molecular junctions, various attempts were made. For example, through the introduction of a cross-conjugated system into the DAE molecule, namely meta-substituted phenyl end groups, the high conductance state was attained and thereby reversible switching in arrays of Au-DAE-Au

junctions was demonstrated [21]. For DAE junctions with graphene electrodes, the unidirectional switching properties could be turned into bidirectional switching by adding alkane groups into both sides of the molecular backbone [7]. This series of studies demonstrates that the side-arms and end-groups, which provide the coupling between the molecule and the electrodes, play an important role in the switching characteristics since they control the energetic alignment between the Fermi level and the current-carrying molecular orbitals as well as the molecular orbitals' linewidth broadening [19, 22].

1.3. Various Photoswitching Phenomena in Large-Area Junctions.

Molecular photoswitching devices have been developed beyond single-molecule junctions to realize large-area molecular junctions based on DAE molecules. Kronemeijer et al. demonstrated reliable bidirectional photoswitching for such large-area molecular junctions processed with SAMs of DAEs, when poly(3,4-ethylenedioxythiophene):poly(styrene sulfonate) (PEDOT:PSS) was used as a top interlayer in addition to Au electrodes [23]. However, in our recent work on slightly modified DAE molecules, we found no optically-induced switching although the junction structure was the same as above [16]. This observation indicates that the mechanisms behind the photoswitching phenomenon in large-area molecular junctions still remains elusive.

1.4. Difference between the Au-DAE-MLG and Au-DAE-rGO moleuclar junctions

We have previously reported the observation of bidirectional photoswitching behavior in DAE molecular junctions fabricated via self-assembly on an Au bottom electrode with a reduced graphene oxide (rGO) top electrode, which can withstand

external mechanical stress [24]. In the present study, we employ multilayer graphene (MLG) as the top electrode in the molecular junction, which shows a superior optical transmittance and higher conductance than that of the rGO electrode. At the same time, however, we find that the junction no longer exhibits the bidirectional switching behavior; instead, the device can only be switched from the OFF to the ON state, i.e., from the open to the closed state of the employed 1,2-bis(2-methyl-5-(4-mercaptophenylethynyl)furan-3-yl)perfluorcyclopent-1-ene DAE. By performing a quantitative analysis in terms of a Landauer coherent transport model, we attribute the unidirectionality mainly to an increased electronic coupling between the closed state of the molecule and the MLG electrode as compared to the situation for rGO.

Chapter 2. Results and Discussion

2.1. Synthesis of MLG

Ni (300 nm)/Ti (20 nm) substrates purchased from Jinsol, Inc. were cleaned respectively in acetone, methanol, 2-propanol, and deionized water with an ultrasonicator for 10 min each. Then, the substrates were loaded into a chemical vapor deposition (CVD) system (Teraleader Co., Korea) and preheated at 500 °C with a 200 sccm stream of Ar/H_2 at 800 Torr for ~30 min to eliminate the oxidized layer on the Ni surface. Afterwards, the MLG films were grown under a gas flow of 15 sccm CH_4 and 20 sccm Ar/H_2 at 20 Torr for 5 min at 900 °C.

2.2. Molecular Junction Fabrication

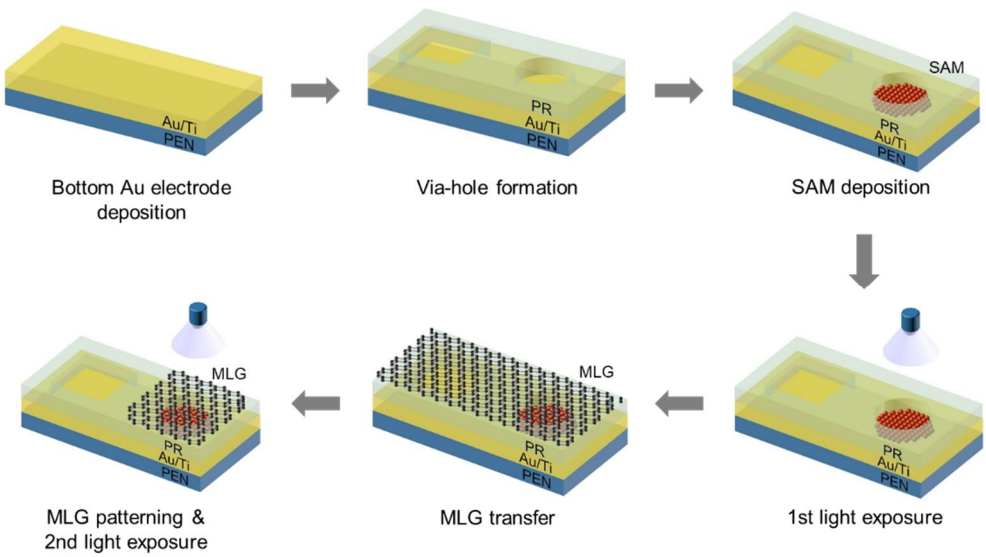

Fig. 2 Schematic representation of the fabrication process for the molecular junctions.

Fig. 2 shows a brief schematic diagram of the fabrication procedure used for the molecular junctions described in this study. We followed the well-established fabrication process that we have previously reported [25-26]. We chose

poly(ethylene-2,6-naphthalate) (PEN) (Q83 purchased from Teijin DuPont Film Co., Ltd.) as a substrate material for the molecular junctions to enable operation even under mechanically flexible conditions. Au (50 nm)/Ti (5 nm) bottom electrodes were deposited onto the PEN substrates at a slow deposition rate of ~0.2 Å/s using an electron beam evaporator. Next, a photoresist (PR) was spin-coated onto the surface, and circular holes with a radius of 10 μm were created on the PR film to expose the surface of the Au electrode by photolithography. The patterned samples were hard-baked at 190 °C for ~2 h to enhance the chemical resistance to the SAM solution. For the SAM deposition, each sample was dipped into a diluted DAE solution (~3 mM in ethanol solvent) for 24 h in a N_2-filled glove box with a few drops of ammonium hydroxide (NH_4OH) added into the solution, which is required to deprotect the acetyl group from the thiol end group. The molecular structure of the DAE under study is illustrated in Fig. 1. Afterwards, we softly rinsed the samples with anhydrous ethanol and exposed each sample to 360 nm UV or 520 nm visible light to induce the closed or open state, respectively. Next, the MLG film was transferred to the molecular layer to make a contact through van der Waals interaction. The detailed procedure for preparing the transfer will be described in the following section. The unnecessary MLG part was removed via a shadow mask by means of an oxygen plasma treatment (under 10 sccm of O_2 gas at 50 W of power) to define each junction. Lastly, we once more exposed each sample to light (UV or visible) to ensure that the molecules remained in the desired state. The entire process after the SAM deposition was conducted in the dark to avoid undesirable effects caused by light exposure. Fig. 3 shows the images of the fabricated molecular junctions obtained from optical microscopy, scanning electron microscopy (SEM), and cross-sectional transmission electron microscopy (TEM). From the atomic composition profile determined from energy-dispersive X-ray spectroscopy (EDS) along the cross section shown in Fig. 3, we could confirm that the C-rich part exists in the MLG and SAM layer between the surrounding Au parts. On the other hand, it was observed that the relative proportion of Au atoms decreased in these layers. This observation indicates that the MLG and SAM layers were well deposited and clearly distinguishable from the Au electrode. The Au

peak at the top reflects an Au protection layer, needed for the EDS measurement and deposited using a focused ion beam process.

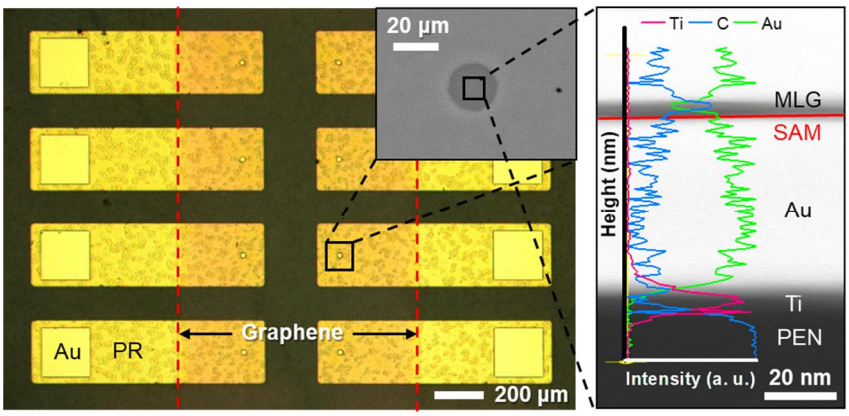

Fig. 3 Optical (left), SEM (inset), and a cross-sectional TEM (right) image of the fabricated molecular junctions. The TEM image is superimposed with an atomic composition profile measured by EDS.

2.3. Preparation of the MLG Top Electrode

The MLG film of the previous section is synthesized on Ni substrates. Subsequently, it is spin-coated with poly(methyl methacrylate) (PMMA, 950PMMA A5 from MicroChem Corp.) as a dummy layer. The Ni layer beneath the MLG film was etched by an iron (III) chloride ($FeCl_3$) aqueous solution. The floating MLG film, detached from the substrate, was rinsed with deionized (DI) water more than three times to eliminate the adhered Fe and Ni ions. Then, the cleaned MLG film was placed onto the molecular layer as the top electrode of the molecular junction. After drying for a few hours to ensure good contact with the molecules, the PMMA layer was removed with acetone and isopropyl alcohol (IPA).

2.4. Electrical Characterization

The electrical characteristics of the molecular junctions were measured with a semiconductor parameter analyzer (Keithley 4200 SCS) and a probe station system (JANIS Model ST-500) under ambient conditions.

Chapter 3. Results and discussion

3.1. Optical and morphological characteristics of the MLG

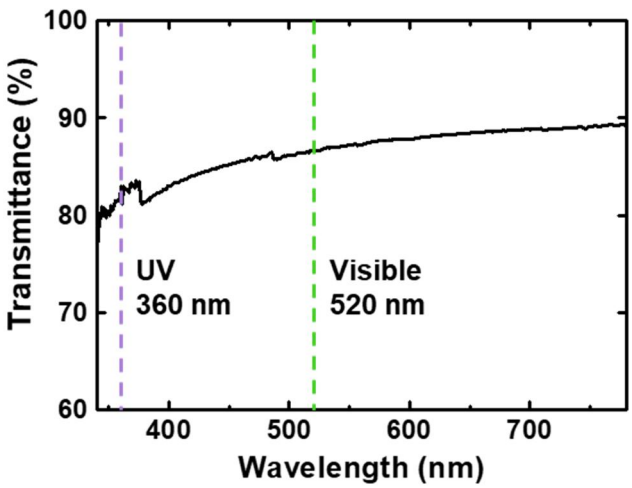

Fig. 4 The measured optical transmittance of a MLG film on a glass substrate.

Fig.4 presents the optical transmittance of the MLG film measured under light illumination over a wavelength range from 340 to 780 nm. Since the MLG film shows a transmittance of more than 80% at both 360 nm and 520 nm, the material can be considered adequately transparent at the wavelengths at which the state of DAE can be transformed.

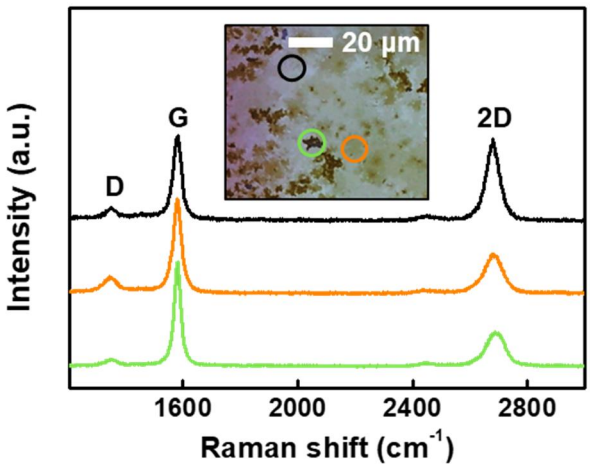

Fig. 5 Raman spectra for three different areas of a MLG film.

The typical D, G, and 2D peaks of the MLG film in the Raman spectrum at energy shifts of 1350, 1580, and 2680 cm^{-1}, respectively, are shown in Fig. 5. The individual colored lines in this graph indicate the Raman peaks for the corresponding areas in the optical microscope (OM) image shown in the inset. The region marked by a black circle in the OM image has similar intensities for the G and 2D peaks in the Raman spectrum (black line). This indicates that the MLG film in that region is relatively thin and can be regarded as triple-layer graphene. On the other hand, the height of the 2D peaks is approximately half of those of the G peaks in the green and orange encircled regions in the OM image, and thus these areas are considered to be thicker multilayers [27].

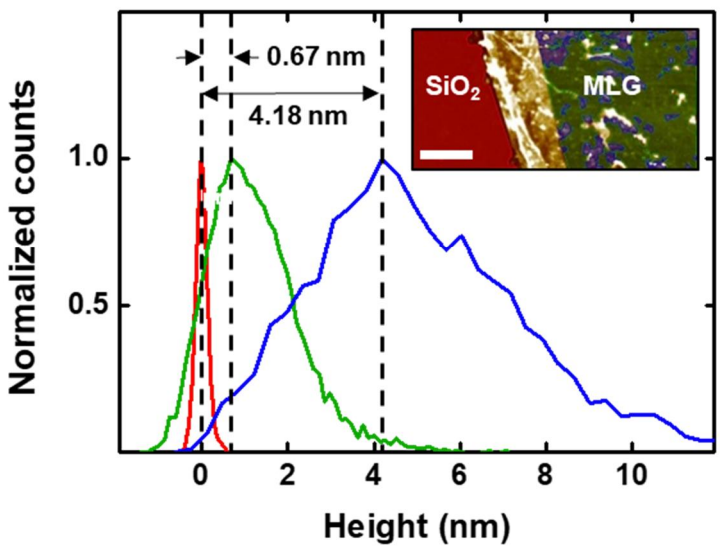

Fig. 6 A topographic profile of a MLG film. The white scale bar in the inset image represents 4 μm.

Fig.6 shows the topographic profile of a MLG film transferred onto a SiO_2/Si substrate. Each colored line in the graph represents the area marked with the same color in the atomic force microscope (AFM) image shown in the inset. The normalized count denotes the number of pixels for a certain height in each area divided by the maximum value of counts as obtained over all heights. This analysis shows that most of the area marked in green in the inset image has a thickness of 0.67 nm, which is similar to that of a monolayer of graphene, and that the small areas marked in blue have a thickness of 4.18 nm. When zooming in on the area of the green region, we find many multilayer features. Therefore, the results are in agreement with earlier reports that the MLG film, grown on a Ni substrate, is non-uniform, rather thick and optically transparent [28].

3.2. Electrical Characteristics of DAE Molecular Junctions with MLG Top Electrode

The *J-V* data were obtained from the open and closed state junctions, fabricated separately.

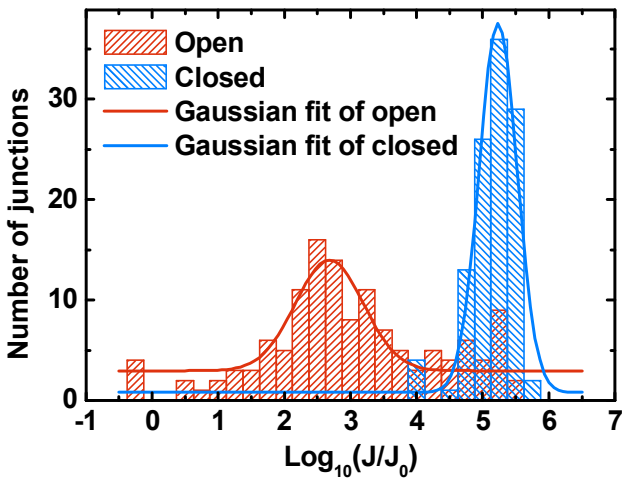

Fig. 7 Histogram of current-density values for all open- and closed-state molecular junctions measured at a bias of $V = 1$ V.

Fig.7 shows the histograms of the current density values for each state measured at 1 V from the entire set of working molecular junctions (131 molecular junctions in the open state and 111 molecular junctions in the closed state). Nonworking molecular junctions can be easily recognized as short-circuited or open-circuited and are excluded [29].

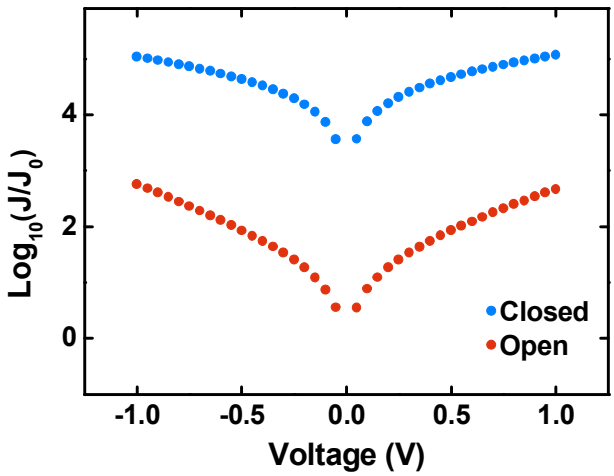

Fig. 8 Representative logarithmic *J-V* curves for the closed and open state DAE molecular junctions.

We defined the maximum of the Gaussian distribution, fitted to the histograms, as the representative current level of each state, as shown in Fig. 8.

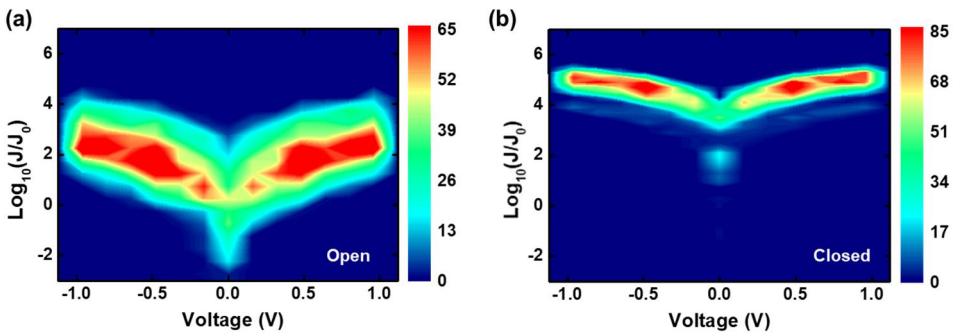

Fig. 9 Two-dimensional logarithmic *J-V* plots for intact molecular junctions in (a) open and (b) closed states. Here, J_0 = 1 A/cm^2 (see the text).

In Fig. 9(a) and 9(b), the two-dimensional *J-V* histograms are depicted as contour plots for all the working open and closed state junctions, respectively. Although the variance of the current level in the open state is larger than that in the closed state, we find that the current levels of the two different states are separated by two orders of magnitude. This means that the molecular junctions with the MLG top

electrode show distinct electrical properties in response to the light, similar to previous reports [24].

3.3. Phototransition Properties of DAE Molecular Junctions.

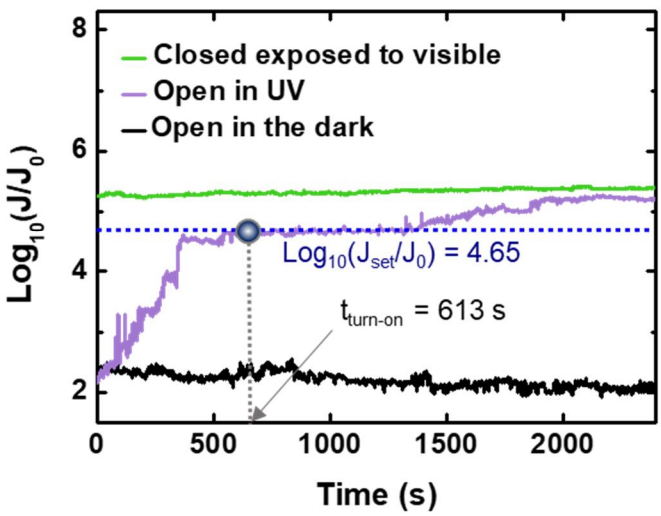

Fig. 10 Real-time measurement of the current density for each state with or without exposure to light at an applied bias voltage of $V = 1$ V. The switching time ($t_{turn\text{-}on}$) is indicted by an arrow.

Subsequently, we examined the phototransition properties of the DAE molecular junctions. Fig. 10 shows real-time current density (*J-t*) measurements for three cases: open state in the dark (black line), open state exposed to 15 mW UV light (purple line), and closed state exposed to visible light (green line) with the same intensity as the UV light. All the measurements were carried out under a constant voltage of 1 V, and the time on the x-axis of the graph was adjusted to start from the point when irradiation was initiated. The current level of the junction in the open state in the dark showed no changes, which suggests that the bias voltage applied to the molecular junction cannot induce the switching. In addition, for the case of the molecular junction prepared in the closed state, the switching behavior could not be observed when exposed to visible light. On the other hand, we observed a unidirectional real-time switching behavior from the open to the closed state under UV light illumination. We defined the switching time as the time to

reach 90% of the average current value at 1 V in the closed state ($\log_{10}(J_{set}/J_0)$ = 4.65 with J_0 = 1 A/cm^2 and J_{set} chosen to be 90% of the average J value, as indicated by the blue arrow in Figure 3a). The switching time of the representative molecular junction for the open state to transition to the closed state upon exposure to UV light was found to be 613 s (indicated as $t_{turn\text{-}on}$ in Fig. 10).

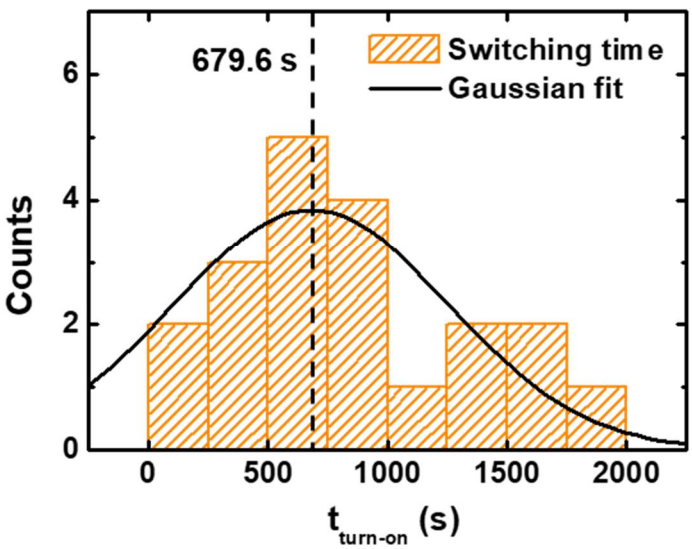

Fig. 11 Histogram for the measured switching time required to transition from the open to the closed state. The Gaussian fit to the histogram is shown by the solid line, and the average switching time is shown by the dashed line.

The switching times obtained from 21 different molecular junctions (Fig. 12) were distributed as shown in Fig. 11. The average switching time for these 21 molecular junctions was determined to be around 680 s by performing a Gaussian fit to the statistical data, as shown in Fig. 11.

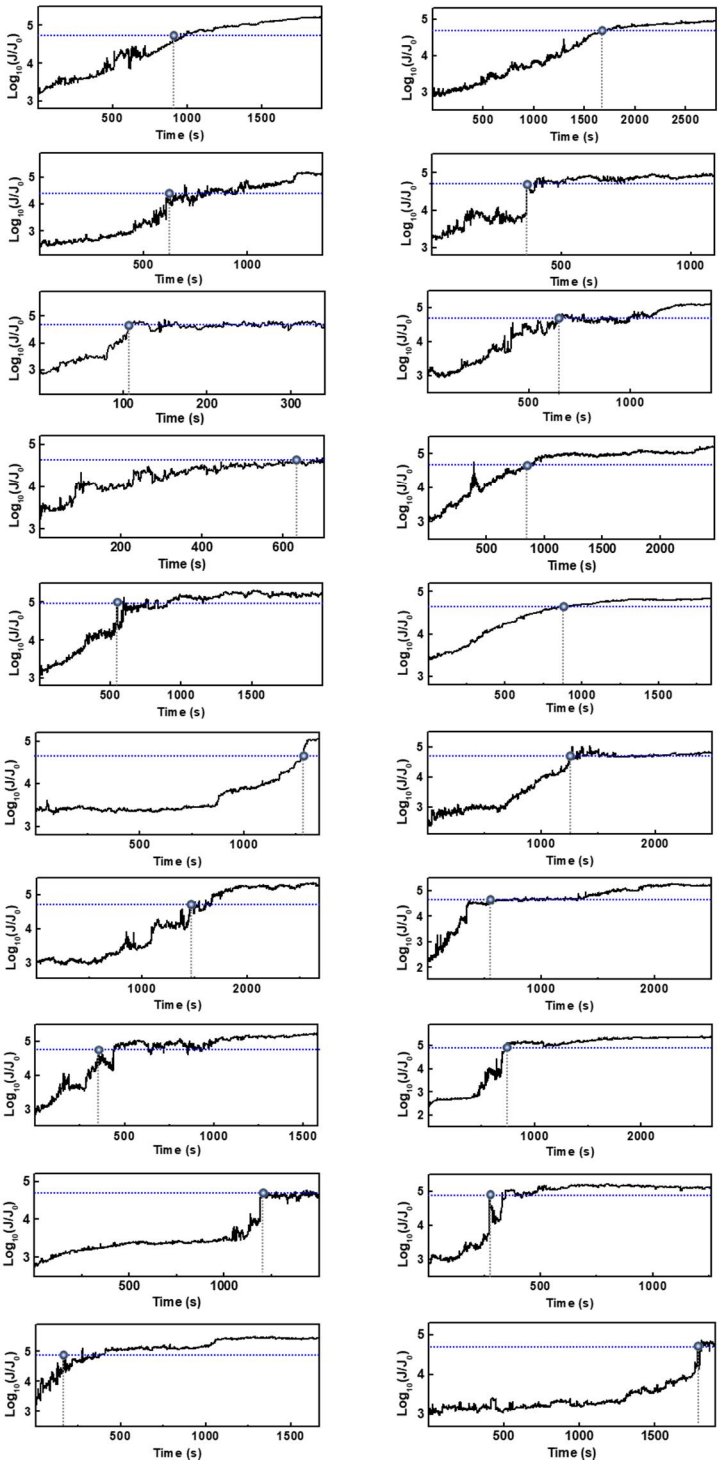

Fig. 12 Real-time measurements of switching from the open to the closed state.

3.4. Landauer Formula

To gain a better understanding of the charge transport through the molecular junctions and to investigate the unidirectional switching behavior, we apply the Landauer formalism [30]. We approximate the current through an equivalent single-molecule junction as

$$I_{\text{single}} = \frac{c}{NA} I_{\text{exp}} = \frac{2e}{h} \int_{-\infty}^{\infty} T(E)[f_1(E) - f_2(E)]dE. \quad (1)$$

In Eq. (1), $f_X(E) = (1 + \exp((E - \mu_X)/k_B T))^{-1}$ is the Fermi-Dirac distribution function, where μ_X is the chemical potential of the electrode X = top or bottom, and $T(E)$ is the transmission function with a Lorentzian shape around the molecular orbital (MO) n described as

$$T(E) = \sum_n \frac{4\Gamma_{\text{n,top}}\Gamma_{\text{n,bottom}}}{[\Gamma_{\text{n}}{}^2 + (E - E_n)^2]}. \quad (2)$$

Here $\Gamma_{n,X}$ indicates the electronic coupling strength of the MO n to the respective electrode X, and $\Gamma_{\text{n}} = \Gamma_{\text{n,top}} + \Gamma_{\text{n,bottom}}$ defines the total linewidth broadening. Counting all energies from the Fermi energy E_{F} as the reference, E_{n} is the difference between the eigenenergy of the MO and the Fermi energy of the electrodes $\mu_X \approx E_{\text{F}}$.

3.5. Simple Calculation for Single Molecule Analysis

Since our system consists of many molecules, we calculate the current per molecule I_{single} by dividing the experimentally measured current I_{exp} by the number of molecules NA in the junction. Here, we choose the coverage N as 4.4×10^{14} cm^{-2} and 5.4×10^{14} cm^{-2} for the closed-state and open-state DAE, respectively [23]. The reason why the packing density of the closed state is lower than the open state is because the energetically most favorable packing and tilt angle (i.e., the optimized molecular conformations that minimize their free energy) is different for the closed-state and open-state [23]. As mentioned above, the area A

of the molecular junctions is approximately 314 μm^2. Furthermore, we multiplied the current by a phenomenological factor c = 3000, because the current per molecule in SAMs has been found to be about 3000 times lower than that in a single-molecule junction in the case of a conjugated molecular wire [31]. This effect is attributed to the fact that SAMs are more effectively screening the external electric field and provide more paths for molecular heat dissipation as compared to single-molecule junctions. These factors facilitate the tunneling through a single-molecule junction as compared to the SAM system. Finally, since the number of molecules that make electrical contact with both electrodes in large-scale molecular junctions is only a fraction of the total number of molecules, per molecule the contact is less conductive than a single-molecule junction [32].

3.6. Simplification of Landauer Formula

To simplify the analysis of I_{single}, we introduce the following assumptions: (i) The contribution from a single MO n=0 determines the current. (ii) Since the experimental *J-V* characteristics are almost symmetric with regard to bias polarity, we assume that the coupling strength is symmetric, i.e., $\Gamma = \Gamma_{0,\text{top}} + \Gamma_{0,\text{bottom}}$ and $\Gamma_{0,\text{top}} = \Gamma_{0,\text{bottom}}$. (iii) The energy level E_0 of the SAM system is fixed, when a bias voltage is applied between the two electrodes. By adopting these assumptions, Equation (2) reduces to

$$T(E) = \frac{\Gamma^2}{[\Gamma^2+(E-E_n)^2]}, \tag{3}$$

where the charge injection barrier is given as $E_0 = E_{\text{HOMO}} - E_{\text{F}}$ or $E_0 = E_{\text{LUMO}} - E_{\text{F}}$ with E_{HOMO} and E_{LUMO} being the energy level of the highest occupied molecular orbital (HOMO) and the lowest unoccupied molecular orbital (LUMO), respectively.

3.7. Approximation for Symmetric Single Model

Let us note that with all these approximations, we use a very simple model to analyze the charge transport through the complex Au-DAE-MLG systems. Indeed the symmetric single-level model appears to be oversimplified, given that junctions are structurally asymmetric. Thus, we expect that the DAE molecules exhibit a weak physical contact to MLG and a strong covalent bond to Au, making it necessary to distinguish between the two couplings $\Gamma_{0,\mathrm{bottom}}$ and $\Gamma_{0,\mathrm{top}}$. However, the couplings also significantly depend on the intramolecular coupling strength between the central part of the molecule and the contact groups at the ends [33]. Indeed, Nijhuis and collaborators showed that both *J-V* curves as well as $\Gamma_{0,\mathrm{bottom}}$ and $\Gamma_{0,\mathrm{top}}$ are almost symmetric for ferrocenyl-based molecules between one covalently bound and one physisorbed contact, when the ferrocenyl unit was located at the center of the molecule [34]. We therefore hope that the effective parameters Γ and E_0, extracted from the single-level model, yield meaningful trends. Let us also point out that only the absolute value of E_0, i.e. $|E_0|$, can be determined from current-voltage characteristics. To simplify the notation, we will omit the symbol for the absolute value in the following, and assume that $E_0 \geq 0$.

3.8. Fitting Results and Implications of DAE molecular Junctions with MLG Electrode

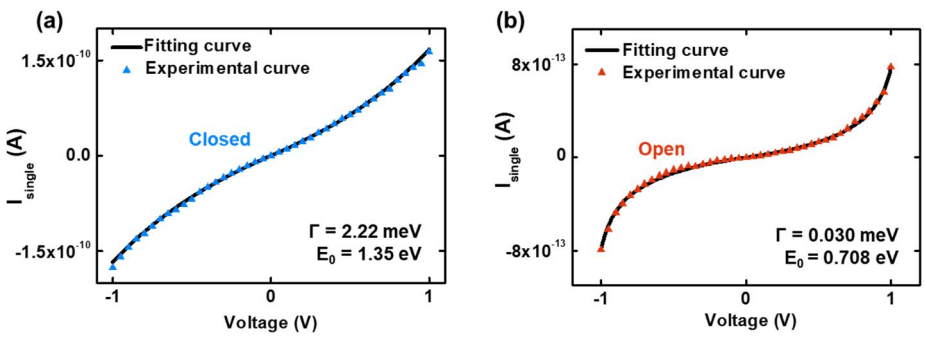

Fig. 13 A representative I_{single}-V curve measured for the (a) closed and (b) open state, with the fitting curve (shown as a solid line) calculated based on the Landauer formula. The

corresponding coupling and level alignment values used in the fits are listed at the bottom right of each graph.

As described in a previous publication [30], we have numerically fitted experimental I_{single}–V curves to estimate Γ and E_0 values by adopting the Levenberg-Marquardt algorithm. Fig. 13(a) and 13(b) show representative I_{single}–V curves and the corresponding fits for the closed and open states. The fits reproduce the measurements well with minimal variation over the whole voltage range. In addition, we conducted the fitting for 91 closed-state and 84 open-state molecular junctions, and then extracted Γ and E_0 values for all the junctions. All the Γ and E_0 values determined are presented in the scatter plot in Fig. 14(a) and 14(b).

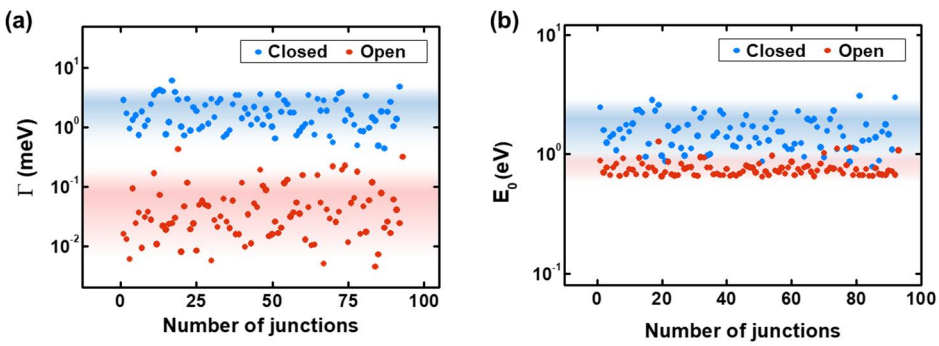

Fig. 14 Scatter point plots for (a) Γ and (b) E_0 values for intact molecular junctions in the closed and open state. The shaded regions represent areas, where the data points deviate by no more than 60% from the averages. Here, Γ values for the closed and open states are clearly separated from each other, while they mix for E_0.

By averaging these distributions, the effective coupling strength Γ for closed and open states was determined to be 1.93 ± 0.12 meV and 0.0572 ± 0.0072 meV, respectively, and the corresponding charge injection barrier E_0 for closed and open states was extracted to be 1.560 ± 0.054 meV and 0.756 ± 0.012 meV, respectively, as summarized in Table 1.

Table 1. Charge injection barrier (E_0) and coupling constant (Γ) as extracted from a set of I_{single}–V curves by using the Landauer formula.

		Γ (meV)	E_0 (eV)
Au – DAE - MLG	Closed	1.93 ± 0.12	1.560 ± 0.054
	Open	0.0572 ± 0.0072	0.756 ± 0.012
Au – DAE - rGO	Closed	0.462± 0.039	2.19 ± 0.18
	Open	0.250 ± 0.040	2.72 ± 0.38

Note that the level alignment E_0 shows a complex behavior opposite to the naive expectation that E_0 in the open state would be higher than for the closed state. This expectation is based on the fact that the electronic gap between the HOMO and the LUMO in an isolated DAE molecule is larger in the open state than in the closed one. Calculations using various levels of ab-initio electronic structure theory are summarized in Table 2 and indeed confirm this assertion.

Table 2. Calculated HOMO-LUMO gap values Δ (DFT, ΔSCF, G_0W_0, evGW) and optical gaps (BSE) of the isolated DAE molecule, as determined from different methods of ab-initio electronic structure theory. The information in brackets in the method column specifies details of the calculations such as the basis set, the exchange correlation functional (for DFT and ΔSCF calculations) as well as which geometries and level of theory was used as a starting value in the post-DFT procedures (G_0W_0, evGW, BSE).

Method	Closed (eV)	Open (eV)
DFT (BP86, def-SV(P))	1.04	2.32
DFT (PBE, def-SV(P))	1.04	2.36
DFT (PBE, def-TZVP)	1.07	2.24
ΔSCF (PBE, def2-TZVP)	3.89	5.05
G_0W_0 (PBE, def2-TZVP)	5.59	5.75
evGW (PBE, def2-TZVP)	4.20	6.61
BSE (evGW, PBE, def2-TZVP)	1.67	3.62

It is also apparent from the expression for the transmission in Equation (3) that the difference in Γ values between closed and open states determines the magnitude of current rather than the difference in E_0 values. In particular, it is notable that the effective value of Γ in the closed state is more than 30 times larger than that of the open state, while E_0 differs only by a factor of around 2. Thus, the Γ values explain, why the closed state is more conductive than the open one.

In addition to a previous explanation that the small quantum yield of the ring opening reaction reduces the switching rate [19], the relatively strong coupling between DAE and MLG electrodes in the closed state may also cause the unidirectional switching. It is possible that the strong interaction between the closed state of the DAE molecules and the electrode can quench the photoexcited closed state, effectively disturbing the switching process and eventually preventing the transition to the open state [17, 35-36].

3.9. Fitting Results and Implications of DAE molecular Junctions with rGO Electrode

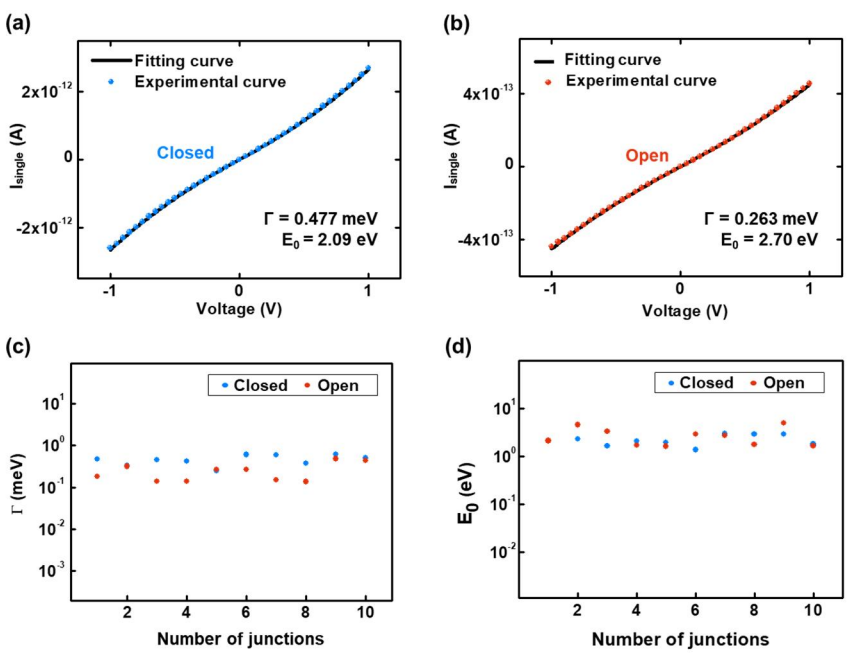

Fig. 15 A few examples of I_{single}-V curves and the corresponding fits for open and closed states of Au-DAE-rGO molecular junctions.

We also applied the same method to analyze the measurement data for Au-DAE-rGO junctions reported in our previous work [24]. In Fig. 15(a) and 15(b), representative fitting results are shown for closed and open states, both of which were well-fitted. The averaged fitting results, obtained from ten Au-DAE-rGO junctions, are given in Table 1. The extracted Γ values for closed and open states were calculated as 0.462 ± 0.039 meV and 0.250 ± 0.040 meV, respectively, both of which are roughly one order lower than the value obtained for the closed state in Au-DAE-MLG junctions. The effective E_0 values for closed and open states were found to be 2.19 ± 0.18 meV and 2.72 ± 0.38 meV, respectively. As depicted in Fig. 15(c), the distribution of Γ values for both states in Au-DAE-rGO junctions is in a similar range within one order, in contrast to the Au-DAE-MLG junctions which showed a significant difference in electronic couplings between closed and open states. Level alignments E_0 between open and closed junctions in Fig. 15(d) practically do not differ. This result corroborates that bidirectional switching in Au-DAE-rGO junctions correlates well with similar and small Γ values for both closed and open states.

The different tendency of the Γ values in the Au-DAE-MLG junctions compared to those in the Au-DAE-rGO junctions can reasonably explain, why the former junctions show unidirectional switching, whereas the latter exhibit bidirectional switching. Our analysis reveals that the interaction between the molecules and the electrodes is important not only for the current level but also for the directionality of the switching behavior. We conclude that the interaction between the DAE molecules and different electrode materials can lead to drastically different device characteristics.

Chapter 4. Conclusion

In summary, we fabricated and characterized DAE photoswitching molecular junctions using Au bottom and MLG top electrodes. We found clearly distinguishable electrical properties for the molecular junctions between closed and open states with average current levels differing by two orders of magnitude. At the same time we found in real-time measurements that the junctions exhibited a unidirectional switching behavior from the open to the closed state. To better understand the unidirectionality, we extracted electronic coupling and level alignment parameters, Γ and E_0, by fitting experimental *J-V* curves with the Landauer formula. The calculated Γ value for the Au-DAE-MLG junctions in the closed state was significantly larger than in the open state. A comparison with previously measured Au-DAE-rGO junctions, which show bidirectional switching, revealed that the electronic couplings Γ correlate well with the photoswitching behavior and not the level alignment. By relating the electronic measurements with photoswitching device characteristics, we thus attribute the inability to switch to the open state to the strong coupling between DAE and the MLG electrode in the closed state together with the low quantum yield of the opening reaction. Our study suggests that the electronic coupling between molecules and electrodes plays a significant role for any molecular photoswitching device.

Bibliography

[1] Bumm, L. A.; Arnold, J. J.; Cygan, M. T.; Dunbar, T. D.; Burgin, T. P.; Jones, L.; Allara, D. L.; Tour, J. M.; Weiss, P. S., Are Single Molecular Wires Conducting? *Science* **1996,** *271*, 1705-1707.

[2] Wold, D. J.; Haag, R.; Rampi, M. A.; Frisbie, C. D., Distance Dependence of Electron Tunneling through Self-Assembled Monolayers Measured by Conducting Probe Atomic Force Microscopy: Unsaturated versus Saturated Molecular Junctions. *J. Phys. Chem. B* **2002,** *106*, 2813-2816.

[3] Tanaka, T.; Osuka, A., Conjugated Porphyrin Arrays: Synthesis, Properties and Applications for Functional Materials. *Chem. Soc. Rev.* **2015,** *44*, 943-969.

[4] Aviram, A.; Ratner, M. A., Molecular Rectifiers. *Chem. Phys. Lett.* **1974,** *29*, 277-283.

[5] Chen, X.; Roemer, M.; Yuan, L.; Du, W.; Thompson, D.; del Barco, E.; Nijhuis, C. A., Molecular Diodes with Rectification Ratios Exceeding 10^5 driven by Electrostatic Interactions. *Nat. Nanotechnol.* **2017,** *12*, 797-803.

[6] Osorio, E. A.; Moth-Poulsen, K.; van der Zant, H. S. J.; Paaske, J.; Hedegård, P.; Flensberg, K.; Bendix, J.; Bjørnholm, T., Electrical Manipulation of Spin States in a Single Electrostatically Gated Transition-Metal Complex. *Nano Lett.* **2009,** *10*, 105-110.

[7] Jia, C.; Migliore, A.; Xin, N.; Huang, S.; Wang, J.; Yang, Q.; Wang, S.; Chen, H.; Wang, D.; Feng, B., Covalently Bonded Single-Molecule Junctions with Stable and Reversible Photoswitched Conductivity. *Science* **2016,** *352*, 1443-1445.

[8] Song, H.; Kim, Y.; Jang, Y. H.; Jeong, H.; Reed, M. A.; Lee, T., Observation of Molecular Orbital Gating. *Nature* **2009,** *462*, 1039-1043.

[9] Capozzi, B.; Chen, Q.; Darancet, P.; Kotiuga, M.; Buzzeo, M.; Neaton, J. B.; Nuckolls, C.; Venkataraman, L., Tunable Charge Transport in Single-Molecule Junctions via Electrolytic Gating. *Nano Lett.* **2014,** *14*, 1400-1404.

[10] Cui, L.; Miao, R.; Wang, K.; Thompson, D.; Zotti, L. A.; Cuevas, J. C.; Meyhofer, E.; Reddy, P., Peltier Cooling in Molecular Junctions. *Nat. Nanotechnol.* **2018,** *13*, 122-127.

[11] Seo, S.; Min, M.; Lee, S. M.; Lee, H., Photo-Switchable Molecular Monolayer Anchored between Highly Transparent and Flexible Graphene Electrodes. *Nat. Commun.* **2013,** *4*, 1920.

[12] Hagen, S.; Leyssner, F.; Nandi, D.; Wolf, M.; Tegeder, P., Reversible Switching of Tetra-Tert-Butyl-Azobenzene on a Au (1 1 1) Surface Induced by Light and Thermal Activation. *Chem. Phys. Lett.* **2007,** *444*, 85-90.

[13] Alemani, M.; Peters, M. V.; Hecht, S.; Rieder, K.-H.; Moresco, F.; Grill, L., Electric Field-Induced Isomerization of Azobenzene by STM. *J. Am. Chem. Soc.* **2006,** *128*, 14446-14447.

[14] Irie, M.; Kobatake, S.; Horichi, M., Reversible Surface Morphology Changes of a Photochromic Diarylethene Single Crystal by Photoirradiation. *Science* **2001,** *291*, 1769-1772.

[15] Whalley, A. C.; Steigerwald, M. L.; Guo, X.; Nuckolls, C., Reversible Switching in Molecular Electronic Devices. *J. Am. Chem. Soc.* **2007,** *129*, 12590-12591.

[16] Kim, D.; Jeong, H.; Lee, H.; Hwang, W. T.; Wolf, J.; Scheer, E.; Huhn, T.; Jeong, H.; Lee, T., Flexible Molecular-Scale Electronic Devices composed of Diarylethene Photoswitching Molecules. *Adv. Mater.* **2014,** *26*, 3968-3973.

[17] Dulic, D.; van der Molen, S. J.; Kudernac, T.; Jonkman, H. T.; de Jong, J. J.; Bowden, T. N.; van Esch, J.; Feringa, B. L.; van Wees, B. J., One-Way Optoelectronic Switching of Photochromic Molecules on Gold. *Phys. Rev. Lett.* **2003,** *91*, 207402.

[18] Zhuang, M.; Ernzerhof, M., Reversibility and Transport Properties of Dithienylethene Photoswitches. *J. Chem. Phys.* **2009,** *130*, 114704.

[19] Sendler, T.; Luka□Guth, K.; Wieser, M.; Wolf, J.; Helm, M.; Gemming, S.; Kerbusch, J.; Scheer, E.; Huhn, T.; Erbe, A., Light□Induced Switching of Tunable Single□Molecule Junctions. *Adv. Sci.* **2015,** *2*, 1500017.

[20] Jia, C.; Wang, J.; Yao, C.; Cao, Y.; Zhong, Y.; Liu, Z.; Liu, Z.; Guo, X., Conductance Switching and Mechanisms in Single-Molecule Junctions. *Angew. Chem., Int. Ed. Engl.* **2013,** *52*, 8666-8670.

[21] van der Molen, S. J.; Liao, J.; Kudernac, T.; Agustsson, J. S.; Bernard, L.; Calame, M.; van Wees, B. J.; Feringa, B. L.; Schoñenberger, C., Light-

Controlled Conductance Switching of Ordered Metal-Molecule-Metal Devices. *Nano Lett.* **2008,** *9*, 76-80.

[22] Zotti, L. A.; Kirchner, T.; Cuevas, J. C.; Pauly, F.; Huhn, T.; Scheer, E.; Erbe, A., Revealing the Role of Anchoring Groups in the Electrical Conduction Through Single□Molecule Junctions. *Small* **2010,** *6*, 1529-1535.

[23] Kronemeijer, A. J.; Akkerman, H. B.; Kudernac, T.; van Wees, B. J.; Feringa, B. L.; Blom, P. W. M.; de Boer, B., Reversible Conductance Switching in Molecular Devices. *Adv. Mater.* **2008,** *20*, 1467-1473.

[24] Kim, D.; Jeong, H.; Hwang, W.-T.; Jang, Y.; Sysoiev, D.; Scheer, E.; Huhn, T.; Min, M.; Lee, H.; Lee, T., Reversible Switching Phenomenon in Diarylethene Molecular Devices with Reduced Graphene Oxide Electrodes on Flexible Substrates. *Adv. Funct. Mater.* **2015,** *25*, 5918-5923.

[25] Jang, Y.; Kwon, S.-J.; Shin, J.; Jeong, H.; Hwang, W.-T.; Kim, J.; Koo, J.; Ko, T.; Ryu, S.; Wang, G., Interface-Engineered Charge-Transport Properties in Benzenedithiol Molecular Electronic Junctions via Chemically p-Doped Graphene Electrodes. *ACS Appl. Mater. Interfaces* **2017,** *9*, 42043-42049.

[26] Kim, J.; Jeong, H.; Seong, S.; Kim, M.; Kim, D.; Hwang, W.-T.; Jang, Y.; Choi, B. Y.; Koo, J.; Park, S. B., Comparative Study for Electrical Transport Characteristics of Self-Assembled Monolayers Formed by Benzenethiol, Cyclohexanethiol, and Adamantanethiol. *Curr. Appl. Phys.* **2017,** *17*, 1459-1464.

[27] Cho, C.-Y.; Choe, M.; Lee, S.-J.; Hong, S.-H.; Lee, T.; Lim, W.; Kim, S.-T.; Park, S.-J., Near-Ultraviolet Light-Emitting Diodes with Transparent Conducting Layer of Gold-Doped Multi-Layer Graphene. *J. Appl. Phys.* **2013,** *113*, 113102.

[28] Reina, A.; Jia, X.; Ho, J.; Nezich, D.; Son, H.; Bulovic, V.; Dresselhaus, M. S.; Kong, J., Large Area, Few-Layer Graphene Films on Arbitrary Substrates by Chemical Vapor Deposition. *Nano Lett.* **2008,** *9*, 30-35.

[29] Kim, T. W.; Wang, G. N.; Lee, H.; Lee, T., Statistical Analysis of Electronic Properties of Alkanethiols in Metal-Molecule-Metal Junctions. *Nanotechnology* **2007,** *18*, 315204.

[30] Kim, Y.; Hellmuth, T. J.; Sysoiev, D.; Pauly, F.; Pietsch, T.; Wolf, J.; Erbe, A.; Huhn, T.; Groth, U.; Steiner, U. E.; Scheer, E., Charge Transport Characteristics of Diarylethene Photoswitching Single-Molecule Junctions. *Nano Lett.* **2012,** *12*, 3736-3742.

[31] Selzer, Y.; Cai, L.; Cabassi, M. A.; Yao, Y.; Tour, J. M.; Mayer, T. S.; Allara, D. L., Effect of Local Environment on Molecular Conduction: Isolated Molecule versus Self-Assembled Monolayer. *Nano Lett.* **2005,** *5*, 61-65.

[32] Li, B.; Famili, M.; Pensa, E.; Grace, I. M.; Long, N. J.; Lambert, C.; Albrecht, T.; Cohen, L., Cross-plane Conductance through a Graphene/Molecular Monolayer/Au Sandwich. *Nanoscale* **2018**, DOI: 10.1039/C8NR06763E.

[33] Moth-Poulsen, K.; Bjørnholm, T., Molecular Electronics with Single Molecules in Solid-State Devices. *Nat. Nanotechnol.* **2009,** *4*, 551-556.

[34] Yuan, L.; Nerngchamnong, N.; Cao, L.; Hamoudi, H.; Del Barco, E.; Roemer, M.; Sriramula, R. K.; Thompson, D.; Nijhuis, C. A., Controlling the Direction of Rectification in a Molecular Diode. *Nat. Commun.* **2015,** *6*, 6324.

[35] Comstock, M. J.; Levy, N.; Kirakosian, A.; Cho, J.; Lauterwasser, F.; Harvey, J. H.; Strubbe, D. A.; Fréchet, J. M. J.; Trauner, D.; Louie, S. G., Reversible Photomechanical Switching of Individual Engineered Molecules at a Metallic Surface. *Phys. Rev. Lett.* **2007,** *99*, 038301.

[36] Gahl, C.; Schmidt, R.; Brete, D.; McNellis, E. R.; Freyer, W.; Carley, R.; Reuter, K.; Weinelt, M., Structure and Excitonic Coupling in Self-Assembled Monolayers of Azobenzene-Functionalized Alkanethiols. *J. Am. Chem. Soc.* **2010,** *132*, 1831-1838.

Abstract

이 논문은 금을 하부 전극으로, multilayer graphene (MLG)를 상부 전극으로 사용하여 diarylethene (DAE)의 self-assembled monolayers (SAMs)으로 이루어진 수직 구조의 분자 접합에 대한 제작과 특성 관찰에 대한 연구 결과이다. DAE 분자 접합은 UV 빛 조사에 의한 높은 전도도의 closed 상태와 가시광선 빛 조사에 의한 낮은 전도도의 open 상태를 지닌다. Au-DAE-MLG 접합 구조에서 두 상태의 전류 값은 약 100배 정도의 차이를 보였다. 하지만 실시간 측정에서는 open에서 closed 상태로 스위칭 되는 현상만을 관찰하였다. 동시에, 한 시간에 가까운 스위칭 시간을 보였던 이전 연구의 Au-DAE-rGO 분자 접합과는 다르게 Au-DAE-MLG 분자 접합은 10분 정도의 현저히 줄어든 스위칭 시간을 보였다. 이러한 결과들을 설명하기 위해서 두 종류의 분자 접합에 간단한 가정들과 Landauer 식을 적용하였다. 이 분석 방법으로 실험으로 얻은 전류-전압 곡선을 잘 재현하였고, 각각의 분자 접합에 대한 DAE 분자와 상부 전극의 상호작용력을 나타내는 커플링 값을 추출해 냈다. 그 결과, Au-DAE-MLG 분자 접합에 대해서는 큰 커플링 값이 나왔고, Au-DAE-rGO 분자 접합에 대해서는 작은 커플링 값이 나왔다. DAE 분자와 MLG 상부 전극간의 강한 상호작용력이 분자의 광 스위칭 현상을 막을 수도 있다고 해석하였다. 반면에, 작은 커플링 값으로 나오는 약한 상호작용력이 Au-DAE-rGO 분자 접합이 양방향으로 스위칭 할 수 있게끔 한다고 해석하였다. 이러한 해석은 Landauer 식을 기반으로 한 전극-분자 상호작호력의 이론적 계산으로 설명할 수 있다.

주요어 : 분자 소자학, 광스위칭, diarylethene, 자가 조립 단분자층, 그래핀 전극
학번 : 2015-22586